Master's Thesis of Science Education

Projection of Global Sea Level Change in 2050 caused by Antarctic and Greenland ice mass variations

남극과 그린란드 얼음 질량 변화에 의한 2050년 전 지구 해수면 변화 추정

August 2022

Graduate School of Science Education
Seoul National University
Earth Science Major

Donghyuck Lee

Projection of Global Sea Level Change in 2050 caused by Antarctic and Greenland ice Mass Variations

남극과 그린란드 얼음 질량 변화에 의한 2050 년 전 지구 해수면 변화 추정

지도 교수 서 기 원

이 논문을 교육학석사 학위논문으로 제출함
2022년 6월

서울대학교 대학원
과학교육과 지구과학 전공
이 동 혁

이동혁의 교육학석사 학위논문을 인준함
2022년 7월

위 원 장 _____ 안 진 호 _____ (인)

부위원장 _____ 서 기 원 _____ (인)

위 원 _____ 김 병 훈 _____ (인)

Abstract

Global mean sea-level rise is one of the most significant consequences associated with global warming. Because sea-level rise has been mostly determined by ice mass loss in Antarctica and Greenland, it is critical to estimate future ice mass loss from Antarctic and Greenland ice sheets. Several ice sheets models predict ice mass balance from both ice sheets and subsequent sea-level changes with significant model-to-model disagreements. In this study, we projected ice mass variations over both ice sheets up to 2050 based on linear trends and acceleration components in historic ice discharge estimates assuming that ice dynamics would be rather constant during a few decades. Ice discharge components were estimated from observed ice mass variations with surface mass balance (SMB) correction. Future SMB contribution was also included using future projection climate models. We found that future global sea-level rise rate due to AIS would be 0.79~0.99 mm/yr and GrIS would be 0.72 ~ 0.96 mm/yr. AIS contribution to future sea-level rise is similar to or slightly larger than GrIS. Large discrepancies in SMB projections due to climate model uncertainties are the main limitation in this study.

Keyword: Ice Mass Balance, Antarctica, Greenland, Climate Model, Sea-Level Projection

Student Number: 2020-21076

Table of Contents

List of Figure

List of Table

Chapter 1. Introduction

Sea level rise is one of the most critical consequences of ongoing global climate warming. From 1993 to 2015, the global mean sea level (GMSL) has increased at a rate of ~3.1 mm/yr, which has recently accelerated to about 3.5 mm/yr (2005-2015) (Kim et al., 2019). Sea level change is caused mainly by density change associated with thermal expansion and salinity change, and ocean mass change resulting from water mass inflow from land to oceans (Llovel et al., 2019). Among those factors, ocean mass increase is a dominant contributor (Chen et al., 2017) that explains about 67% of global mean sea level rise (GMSL) during 2004-2015 (Kim et al., 2019). Ocean mass increase is mainly caused by ice and water mass inflow to oceans from Antarctic Ice Sheet (AIS), Greenland Ice Sheet (GrIS), mountain glaciers (MG), and terrestrial water storage (TWS) (Llovel et al., 2019). Among them AIS and GrIS are the main contributors to sea level rise (Masson-Delmotte et al., 2021) and thus it is important to understand future AIS and GrIS mass changes for future projection of sea level rise.

Many ice sheet models predict future AIS and GrIS mass change, but there are significant model-to-model discrepancies. For example, GrIS contribution to GMSL rise would range from 40 to 130 mm until 2100 under RCP 8.5 scenario (Goelzer et al. (2020)). At the same forcing scenario, contribution of AIS to GMSL would be from -76 to 300 mm (Seroussi et al., 2020). Such large scattered GrIS projections are mainly caused by uncertainties in initial state of glacier models and low-resolution gridded data (Goelzer et al., 2020). Even

larger discrepancies in AIS projections are due to imperfect representation of glacier models and uncertain boundary conditions (Seroussi et al., 2020).

Instead of using numerical models, AIS and GrIS mass change can be projected empirically assuming that current trends in AIS and GrIS mass change would continue in the near future up to next several decades (Diener et al., 2021). However, because observed ice mass balance includes signals with various time scales, without correction of shorter time scale variations, it is difficult to recover long-term components of ice mass balance (Wouters et al., 2019) and thus to estimate accurate projection of AIS and GrIS mass change. Ice sheet mass balance is composed of surface mass balance (SMB) and ice discharge (D) (Seo et al., 2015). SMB is accumulation of precipitation minus meltwater runoff and sublimation (Van Wessem et al., 2014) while D is ice mass flux into the ocean affected by ocean circulation, basal melting, and grounding line migration (Mouginot et al., 2019). Short-term temporal fluctuation of AIS and GrIS mass balance (detrended mass balance) is usually explained by the seasonal and inter-annual variations in SMB (Shepherd et al., 2020; van den Broeke et al., 2009). By contrast, decadal and longer variability of ice mass balance is generally governed by D (Kim et al., 2020; Shepherd et al., 2018). Therefore, it is reasonable to assume that trends in present D would continue during the next several decades and is used to project future ice mass changes.

Recently, Ice Sheet Mass Balance Inter-Comparison Exercise (IMBIE) reported accurate monthly ice mass balance over both ice sheets since 1992. IMBIE combined multiple remote sensing and numerical models to estimate ice mass variations in AIS and GrIS. Regional Atmospheric Climate Model (RACMO) and Modèle

Atmosphérique Régionale (MAR) also successfully depicts present-day SMB over both ice sheets (Mankoff et al., 2021; Noël et al., 2018; Wessem et al., 2018). The difference between ice mass balance from IMBIE and SMB represents ice discharge, D. In this study, linear trend and acceleration terms were estimated from D time series, and projection of future variations of D was estimated from the two terms. We also considered future SMB from climate models and combined them with D for future ice mass change in both ice sheets. By summing up the mass changes in AIS and GrIS, we estimated both GMSL rise and regional sea level change considering varying Earth's geopotential associated with ice mass redistribution.

Chapter 2. Background

2.1. Ice sheet mass balance

Net mass change in an ice sheet is ice sheet mass balance that is determined by two major processes, SMB and ice discharge (Hanna et al., 2013). Figure 1 shows various processes affecting ice sheet mass balance. Red dots and blue vertical dots in Figure 1 show regions where SMB and ice discharge are occurred.

SMB is ice mass exchange processes on the surface of ice sheets. Major components of SMB are accumulation due to snowfall and ablation due to melting. Both accumulation and ablation are important in Greenland SMB (Seo et al., 2015). In the case of Antarctica, SMB is only approximated to accumulation of snowfall (Seo et al., 2015). This is because, Greenland is vulnerable to surface melting driven by relatively high temperature. In contrast, meltwater runoff in Antarctica is negligible due to low temperature (Lenaerts et al., 2012). Variations of ice discharge is mostly determined by ice flow velocity changes due to the interaction between ice sheets and oceans. Changes in ice flow velocity cause variations of solid ice discharge flux at the grounding line, region where ice sheet contacts with oceans (Hanna et al., 2020). Dashed lines in Figure 1 represent ice flow lines.

Due to the sparse in-situ observation of polar region, SMB can be obtained from regional climate models which are usually forced by reanalysis datasets. Ice discharge in the polar region can be estimated by multiplying the ice flow velocity observed by radar remote sensing to the ice thickness at grounding lines from in-situ observation. Ice

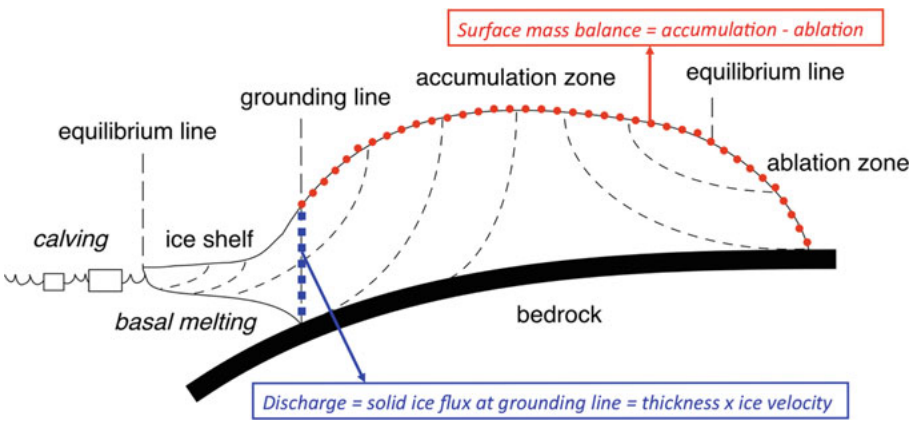

Figure 1. Schematic image of ice sheet and surrounding system. Dashed lines represent approximate ice flow lines. Red dots represent surface of grounded ice where surface mass balance (SMB) is occurred and blue dots are cross-section of the grounding line (from van den Broeke & Giesen, (2021)).

discharge also can be estimated indirectly by differencing between ice mass observation (from satellite gravimetry or altimetry) and modeled SMB.

2.2. Sea-level equation

The present-day mass changes in the Earth's surface affect both the vertical pressure exerted on the surface and the gravitational potential of the surrounding area (Farrell & Clark, 1976; Mitrovica et al., 2001). The former induces vertical displacement due to the elastic properties of Earth's interior (loading), and the latter causes the redistribution of ocean water (self-attraction). The combined effect of these two mechanisms, self-attraction and loading (SAL), increases as it approaches the center of the changing mass, resulting in the spatially non-uniform anomalies of sea-level change. Previous studies also have referred to this phenomenon as gravitationally self-consistent sea-level change or sea-level fingerprint (SLF). Implementing SLF is essential to investigate the realistic sea-level variability in the future.

The observations of Antarctic and Greenland ice sheet mass balance can be represented by mass densities per unit area [kg/m^2], $\Delta\sigma(\theta,\phi)$, in which θ is east longitude and ϕ is colatitude. Generally, the observed $\Delta\sigma(\theta,\phi)$ on the Earth's surface are provided as spherical harmonics (SH) coefficients, which can be transformed into the mass densities at each grid using the following relation (Wahr et al., 1998):

$$\Delta\sigma(\theta,\phi) = a\rho_w \sum_{n=0}^{\infty}\sum_{m=0}^{n}(\Delta\widehat{c_{nm}}(cosm\phi) + \Delta\widehat{s_{nm}}(sinm\phi))\overline{p_{nm}}(cos\theta)) \quad (1)$$

where a is Earth radius, ρ_w is water density, n and m are degree and order, $\Delta\widehat{c_{nm}}$ and $\Delta\widehat{s_{nm}}$ are SH coefficients, and $\overline{p_{nm}}(cos\theta)$ is

normalized associated Legendre functions. Using $\Delta\widehat{c_{nm}}$ and $\Delta\widehat{s_{nm}}$, we can estimate coefficients of the earth's gravity potential (equation 2) and an additional potential perturbation (equation 3) induced by the elastic response of solid earth (Wahr et al. (1998)):

$$\left[\frac{\overline{c_{nm}}}{\overline{s_{nm}}}\right]_{load} = \left[\frac{3\rho_w}{\rho_E(2n+1)}\right]\left[\frac{\Delta\widehat{c_{nm}}}{\Delta\widehat{s_{nm}}}\right] \tag{2}$$

$$\left[\frac{\overline{c_{nm}}}{\overline{s_{nm}}}\right]_{soild\ Earth} = \left[\frac{3\rho_w k'_n}{\rho_E(2n+1)}\right]\left[\frac{\Delta\widehat{c_{nm}}}{\Delta\widehat{s_{nm}}}\right] \tag{3}$$

where, ρ_E is density of the Earth (~5517 kg m^{-3}) and k'_n is load love number. The total potential anomaly induced by mass loads can be estimated by summing up equation (2) and (3).

$$\left[\frac{\overline{c_{nm}}}{\overline{s_{nm}}}\right]_{total} = \left[\frac{\overline{c_{nm}}}{\overline{s_{nm}}}\right]_{load} + \left[\frac{\overline{c_{nm}}}{\overline{s_{nm}}}\right]_{soild\ Earth} = \left[\frac{3\rho_w(1+k'_n)}{\rho_E(2n+1)}\right]\left[\frac{\Delta\widehat{c_{nm}}}{\Delta\widehat{s_{nm}}}\right] \tag{4}$$

Meanwhile, the Earth geoid changes, $\Delta N(\theta,\phi)$, can be represented as follows (Wahr et al., 1998):

$$\Delta N(\theta,\phi) = a\sum_{n=0}^{\infty}\sum_{m=0}^{n}(\Delta\overline{c_{nm}}(cosm\phi) + \Delta\overline{S_{nm}}(sinm\phi))\overline{p_{nm}}(cos\theta)) \tag{5}$$

Substituting the SH coefficients in equation (1) to equation (5), we obtain:

$$\Delta N(\theta,\phi) = \frac{3\rho_w}{\rho_E}\sum_{n=0}^{\infty}\sum_{m=0}^{n}\frac{1+k'_n}{2n+1}(\Delta\widehat{c_{nm}}(cosm\phi) + \Delta\widehat{s_{nm}}(sinm\phi))\overline{p_{nm}}(cos\theta)) \tag{6}$$

Using equation (6), we can estimate geoid anomalies from surface mass densities, such as Antarctic and Greenland ice mass observations. To compute ocean mass change induced by the gravity perturbation from mass changes on the land, we define ocean function $O(\theta,\phi)$, which is 1 over the oceans and 0 over the land. The total land mass change can be estimated by summing up all land grids:

$$\Delta m = \iint \Delta\sigma(\theta,\phi)\big(1 - O(\theta,\phi)\big)\, a^2 d\Omega \tag{7}$$

where $d\Omega$ is surface element $sin\theta d\theta d\phi$. Supposing that all of the land mass loss (Δm) is added into ocean, the mean sea-level change ($\Delta C(\theta,\phi)$) should be:

$$\Delta C(\theta,\phi) = \frac{-\Delta m}{A_o\rho_w}O(\theta,\phi) \tag{8}$$

where A_o means area of total ocean, and ρ_w is density of water (1000 kg/m^3). Adding equation (8) to the geoid anomalies on the ocean ($\Delta N(\theta,\phi)O(\theta,\phi)$) we obtain sea-level fingerprints (ΔS) induced by land mass variation:

$$\Delta S(\theta,\phi) = \Delta C(\theta,\phi) + \Delta N(\theta,\phi)O(\theta,\phi) - \frac{1}{A_o}\iint \Delta N(\theta,\phi)O(\theta,\phi))\, a^2 d\Omega \tag{9}$$

in which the third term of right-hand side of equation (9) denotes spatial average of geoid anomalies over the ocean.

Chapter 3. Data and Method

3.1. Data

3.1.1. AIS and GrIS mass estimates

IMBIE team was established in 2011 to reconcile ice sheet mass balances obtained from satellite measurements. IMBIE estimated AIS and GrIS mass variations from three different satellite techniques of altimetry, gravimetry, and the input-output method (Shepherd et al., 2018; Shepherd et al., 2020). IMBIE provides monthly datasets of AIS ice mass changes in West AIS (WAIS), East AIS (EAIS) and Antarctic Peninsula (AP), separately, from January 1992 to June 2017. Monthly GrIS ice mass change is also provided from January 1992 to December 2018.

3.1.2. Present-day SMB models

Regional climate models have simulated atmospheric processes in polar regions with a high spatial resolution. To separate the SMB effect from the ice mass change, we used two models; Regional Climate Model (RACMO) and Modèle Atmosphérique Régionale (MAR). RACMO is a model developed by Institute for Marine and Atmospheric research Utrecht (IMAU), which has been updated (RACMO2.3p2) from the previous model versions with more improved SMB representation in AIS and GrIS (Noël et al., 2019; Noël et al., 2015; Van Wessem et al., 2014). RACMO2.3p2 of AIS and GrIS are forced by the European Centre for Medium-Range Weather Forecasts (ECMWF) reanalysis. The spatial resolution of RACMO2.3p2 in AIS and GrIS is 27km and 1km, respectively. MAR is another regional climate

model developed by University of Liège specifically focused on polar regions (Mankoff et al., 2021). Depending on the availability of the latest datasets, we used different versions of models for AIS (MARv3.10) (Mottram et al., 2021) and GrIS (MARv3.11) (Fettweis, 2022). MAR in AIS is forced by ERA-Interim, one of the ECMWF reanalysis and GrIS is forced by ERA5, the most recent reanalysis from ECMWF. The spatial resolution of MAR over AIS and GrIS is 35km and 10km, respectively.

3.1.3. CMIP6 SMB models

To project future mass balance of AIS and GrIS, we used SMB data implemented as part of Coupled Model Intercomparison Project (CMIP). CMIP was organized by Working Group on Coupled Modeling (WGCM) (Eyring et al., 2016) which aims at development and review of coupled climate models. CMIP has been developed to phase 6 (CMIP6) now. In addition to the Representative Concentration Pathways (RCPs) in the CMIP5 project, new future pathways (Shared Socioeconomic Pathways (SSPs)) were developed by CMIP6 project, taking into account the human efforts in response to climate change.

We choose 16 SMB from CMIP6 models that provide all of the data for the historical period (~2015), SSP 126, and SSP 585 scenarios. SSP 126 and 585 are low-end and high-end scenarios among CMIP6 models, respectively. The names of adopted models are as follows: GISS-E2-1-G and GISS-E2-1-H, ACCESS-CM2, ACCESS-ESM1-5, CanESM5, CMCC-CM2-SR5, CMCC-ESM2, GFDL-ESM4, INM-CM4-8, INM-CM5-0, KACE-1-0-G, MIROC6, MPI-ESM1-2-HR, MPI-ESM1-2-LR, MRI-ESM2-0, and TaiESM1.

3.2. Method

Ice sheet mass balance, ($\partial M(t)/\partial t$), is a difference between $SMB(t)$ and $D(t)$ (Mouginot et al., 2019):

$$\frac{\partial M(t)}{\partial t} = SMB(t) - D(t) \tag{10}$$

The integration of Equation (10) yields:

$$\delta M(t) = \int \big(SMB(t) - D(t)\big)\, dt$$

We can also separate $SMB(t)$ and $D(t)$ into long-term means during a reference period (SMB_0 and D_0) and anomalous components ($\delta SMB(t)$ and $\delta D(t)$:

$$\delta M(t) = (SMB_0 - D_0)t + \int \big(\delta SMB(t) - \delta D(t)\big)\, dt \tag{11}$$

in which $\delta SMB(t) = SMB(t) - SMB_0$ and $\delta D(t) = D(t) - D_0$. If the reference period is long enough, both ice sheets are assumed to be dynamically equilibrium during the period (i.e., SMB_0 is equal to D_0) (van den Broeke et al., 2009; Xu et al., 2016). This assumption simplifies the above equation to the following form:

$$\delta M(t) = \int \big(\delta SMB(t) - \delta D(t)\big)\, dt$$

, and

$$-\int \delta D(t)dt = \delta M(t) - \int \delta SMB(t)dt. \quad (12)$$

Previous studies (Seo et al., 2015a; Seo et al., 2015b; Kim et al., 2020) indicated that the sub-decadal variability in ice mass change over AIS and GrIS are mostly explained by SMB variation. Thus, subtracting $\int \delta SMB(t)dt$ from $\delta M(t)$ would leave signals dominated by decadal or longer variabilities.

We tested this idea using the IMBIE ice mass estimates and SMB data from two reanalysis datasets. We set the 30-years reference period for estimating SMB_0 from 1979 to 2008. Figure 2 shows comparison of mass balances over AIS and GrIS. As shown in IMBIE2 reports (Shepherd et al., 2018; Shepherd et al., 2019), evident ice mass loss and its acceleration are found in the ice mass balance ($\delta M(t)$, black lines) of both ice sheets (Figures 2a and 2e). In addition, inter-annual variability is also found, which creates inflection points in 2007 and 2002, respectively, to the ice mass balance of AIS and GrIS.

Blue lines in Figure 2 are $\int \delta SMB(t)dt$ from RACMO2.3p2. Inter-annual variabilities in $\delta M(t)$ are similar to those in SMB for all plots. In particular, the inflection points that appear in $\delta M(t)$ of two polar regions are also shown in the SMB time-series, suggesting that the rapid ice loss accelerations were triggered by abrupt atmospheric process. Red lines in Figure 2 are time-series of ice discharge ($-\int \delta D(t)dt$) estimated by equation (12). Unlike $\delta M(t)$, the apparent acceleration patterns in 2002 and 2007 are greatly suppressed in $-\int \delta D(t)dt$. Figure 3 is the similar to Figure 2 except using SMB from MAR. The same interpretation in Figure 2 is also possible here.

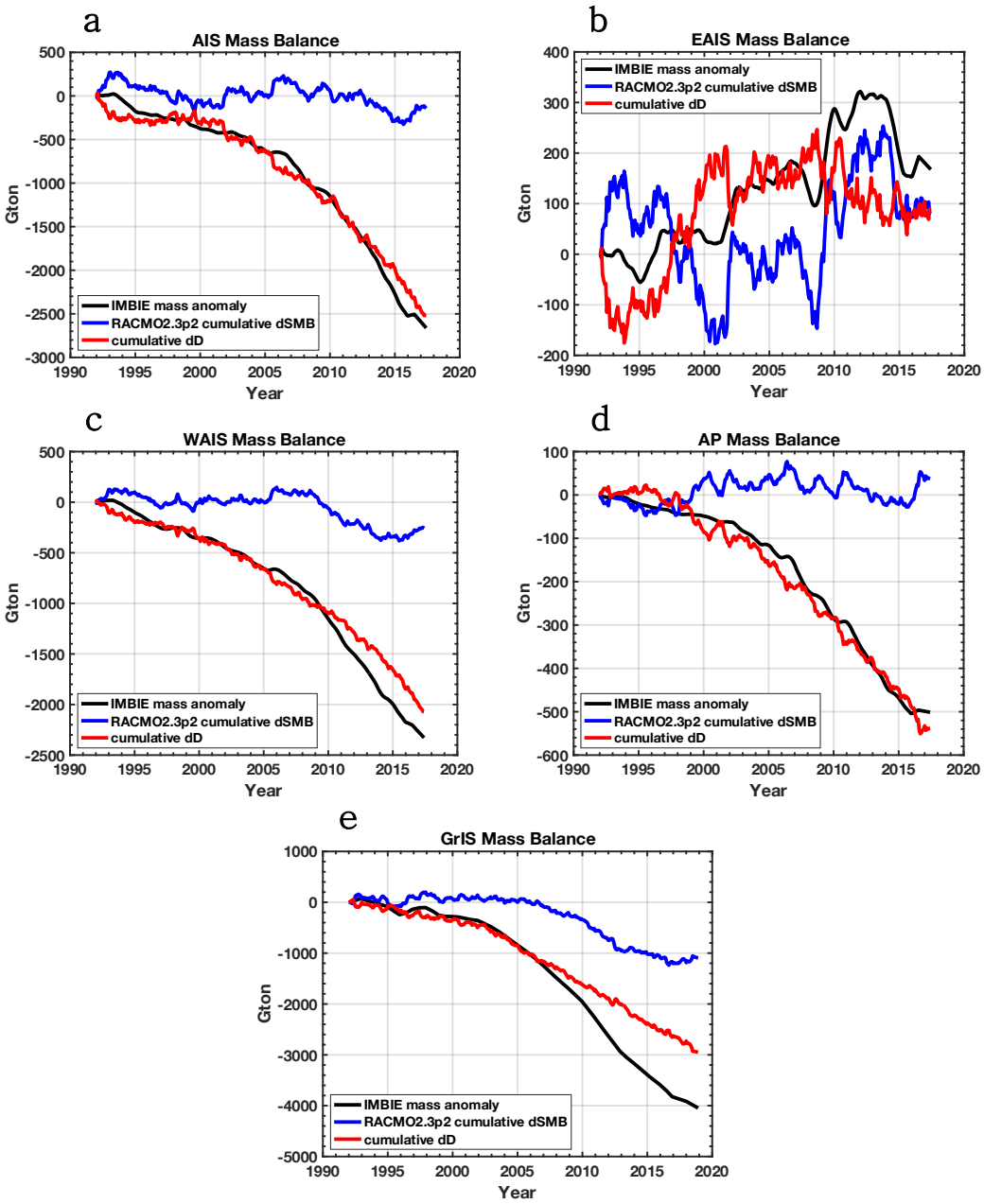

Figure 2. Historical time-series of ice sheet mass balance at AIS (a), EAIS (b), WAIS (c), AP (d) and GrIS (e). Black lines are δM from IMBIE and blue lines are RACMO2.3p2 cumulative δSMB (δSMB = SMB-$SMB_{1979-2008}$) after annual components removed. Red lines are cumulative δD (δD = $SMB_{1979-2008}$-D).

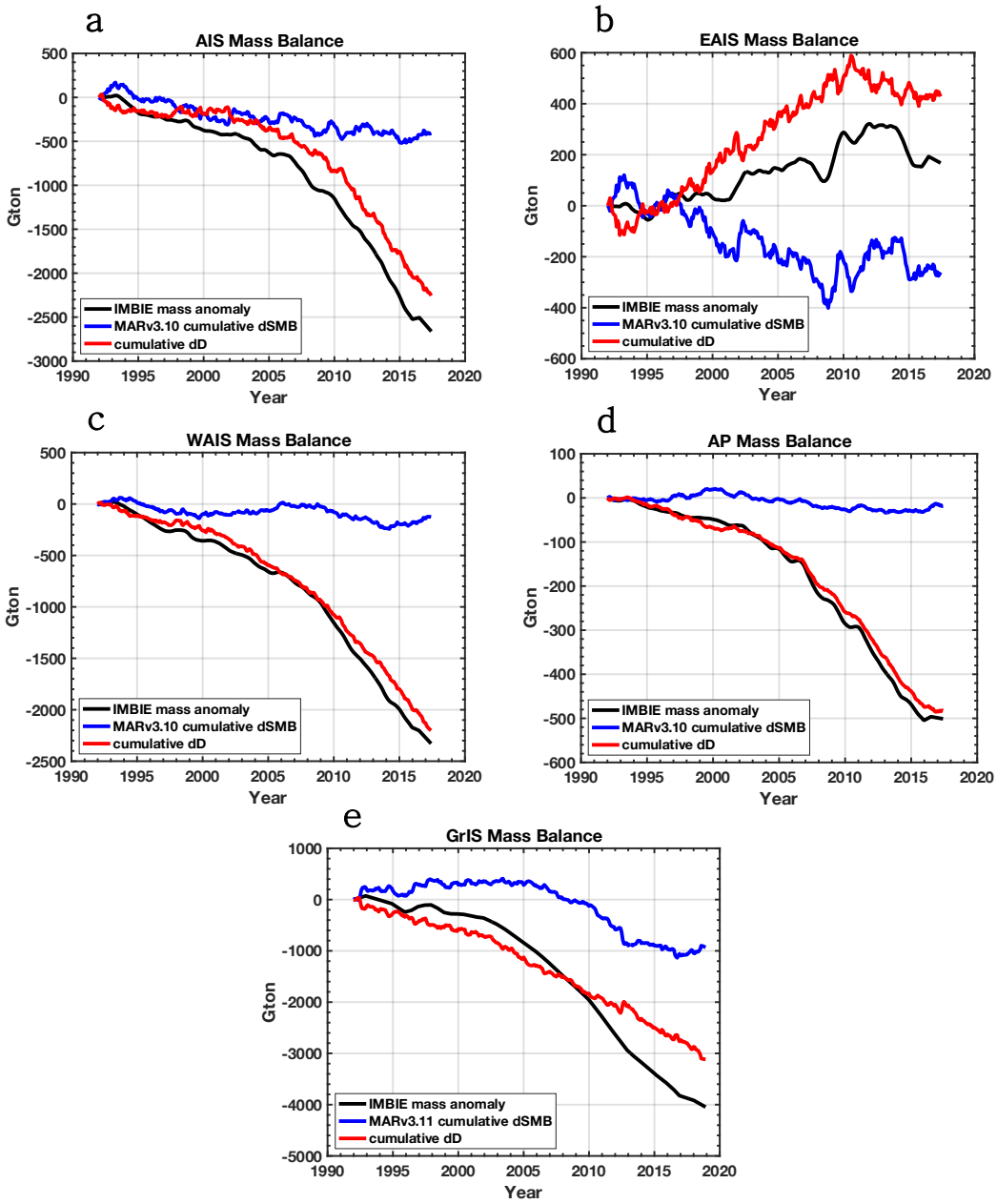

Figure 3. Historical time-series of ice sheet mass balance at AIS (a), EAIS (b), WAIS (c), AP (d) and GrIS (e). Black lines are δM from IMBIE and blue lines are MAR cumulative δSMB (δSMB = SMB-$SMB_{1979-2008}$) after annual components removed. Red lines are cumulative δD (δD = $SMB_{1979-2008}$-D).

Table1 summaries linear trends and accelerations estimated by $\delta M(t)$ and $-\int \delta D(t)dt$. The uncertainties were estimated with 95% confidence intervals. In most cases, the differences in values from $\delta M(t)$ and $-\int \delta D(t)dt$ are statistically significant. Therefore, this experiment demonstrates that simply extrapolating $\delta M(t)$ would cause high uncertainties in future projections of ice mass change due to uncorrected SMB which mostly include inter-annual variabilities.

Unit: [Gton/year]		EAIS	WAIS	AP	GrIS
$\int \delta D$ (RACMO)	Acceleration	-1.43 ± 0.11	-2.42 ± 0.08	-0.72 ± 0.03	-3.18 ± 0.15
	Linear	8.58 ± 0.72	-75.02 ± 0.52	-22.76 ± 0.20	-114.98 ± 1.01
$\int \delta D$ (MAR)	Acceleration	-1.09 ± 0.12	-3.62 ± 0.07	-0.92 ± 0.03	-2.09 ± 0.13
	Linear	25.81 ± 0.82	-83.30 ± 0.46	-19.96 ± 0.20	-113.99 ± 0.88
dM	Acceleration	-0.30 ± 0.12	-3.75 ± 0.15	-1.04 ± 0.35	-6.73 ± 0.28
	Linear	12.64 ± 0.78	-90.39 ± 0.99	-21.48 ± 0.23	-168.17 ± 1.98

Table 1. Accelerations and linear trends (with 95% confidence intervals) estimated by $\delta M(t)$ and cumulative $-\int \delta D(t)dt$. For AIS, the values are estimated from January 1992 to June 2017. For GrIS, the values are estimated from January 1992 to December 2018.

Chapter 4. Projections of Antarctic and Greenland ice mass changes

Using the linear trend and acceleration terms in Table 1, we projected future ice mass changes of AIS and GrIS by 2050 (Figures 4 and 5). Black lines show ice mass balance extrapolated by IMBIE δM and their confidence intervals, with including the contribution of SMB. Ice mass loss in GrIS (Figure 4e) is expected to be the largest, by about −22100 ± 597 Gton. In AIS, ice mass loss of −15949 ± 446 Gton is also expected (Figure 4a) due to the combined effect of mass loss in WAIS (Figure 4c) and AP (Figure 4d). The mass change of EAIS (Figure 4b) is expected to be negligible.

Red lines in Figure 4 show projection of ice discharge extrapolated by using a linear trend and acceleration component in historical estimates of $-\int \delta D(t)dt$ by removing RACMO2.3p2 SMB from IMBIE δM. Compared to the projection of δM, the projected mass loss due to ice discharge is slightly smaller, −14491 ± 312 Gton over AIS (Figure 4a) and −12615 ± 306 Gton over GrIS (Figure 4e). In EAIS, however, the mass loss from ice discharge is expected to be larger than those from IMBIE estimates (Figure 4b), but this contribution is mostly canceled out when integrating the total mass balance over AIS.

To calculate the net mass balance of both ice sheets, we added back the future SMB variations to the projected ice discharge. SMB variations were estimated by ensemble average of 16 CMIP6 models for SSP126 scenario and displayed as cyan lines in Figure 4. 95% confidence intervals were also estimated by two-standard deviations

of 16 model values and were shown as the cyan shadings. The estimates show that increase in AIS SMB would partly compensate for the future ice mass loss (Figures 4a-d). This is because the SMB models predict that increased atmospheric water vapor due to climate warming (Clausius-Clapeyron relation) is likely to cause more snowfall in AIS. On the other hand, SMB in GrIS is expected to be slightly decreased, due to the increased surface melting under the warming climate. Figure 5 is similar to Figure 4 except using SMB associated with SSP 585 scenario.

One important point is that we could not observe a significant difference between the projection of two scenarios (SSP126 and 585) considered in this study, even though more snowfall is predicted in the SSP585 scenario. This is also presumably due to the influence of surface melting. That is, the increased surface melting due to climate warming compensates for most of the increased snowfall in both ice sheet regions.

Combined estimates of projected ice discharge and SMB are presented as green lines in Figures 4 and 5. Green shadings are 95% confidence intervals calculated from uncertainties of both SMB and δM. Uncertainty in SMB is much larger than that in δM. Projections of ice mass balance in 2050 are summarized in Table 2. In any case, this result suggests that our estimates are smaller than those simply projecting historical δM from IMBIE.

Figures 6 and 7 are the similar to Figures 4 and 5 except the case of using MAR SMB to estimate ice discharge variations during the historical period.

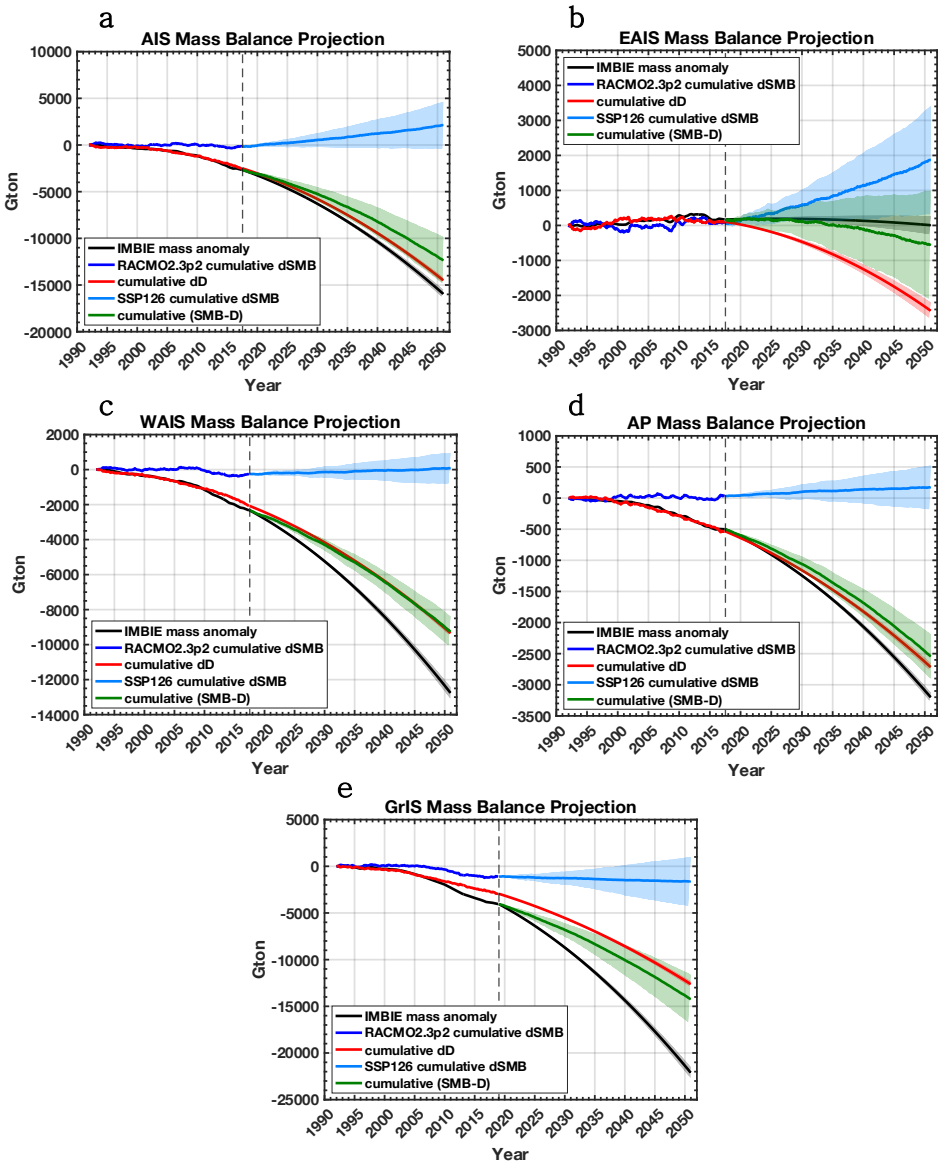

Figure 4. The observed (left side of vertical dashed lines) and projected (right side) ice mass variations in AIS (a), EAIS (b), WAIS (c), AP (d) and GrIS (e). Black lines before dashed lines show net mass balance of ice sheets from IMBIE estimates, and those after dashed lines show projected net mass balance from the extrapolation of IMBIE estimates. The blue lines show SMB variations estimated by RACMO2.3p2, and cyan lines show SMB from CMIP6 models in SSP126 scenario. Red lines before dashed lines are ice discharges estimated by difference of IMBIE estimates and SMB reanalysis. Red lines after dashed lines are ice discharge projected by extrapolation. Green lines are net mass balance estimated in this study. Uncertainties for all graphs are estimated with 95% confidence intervals and are denoted as color shadings. Note that seasonal cycles were removed from SMB models.

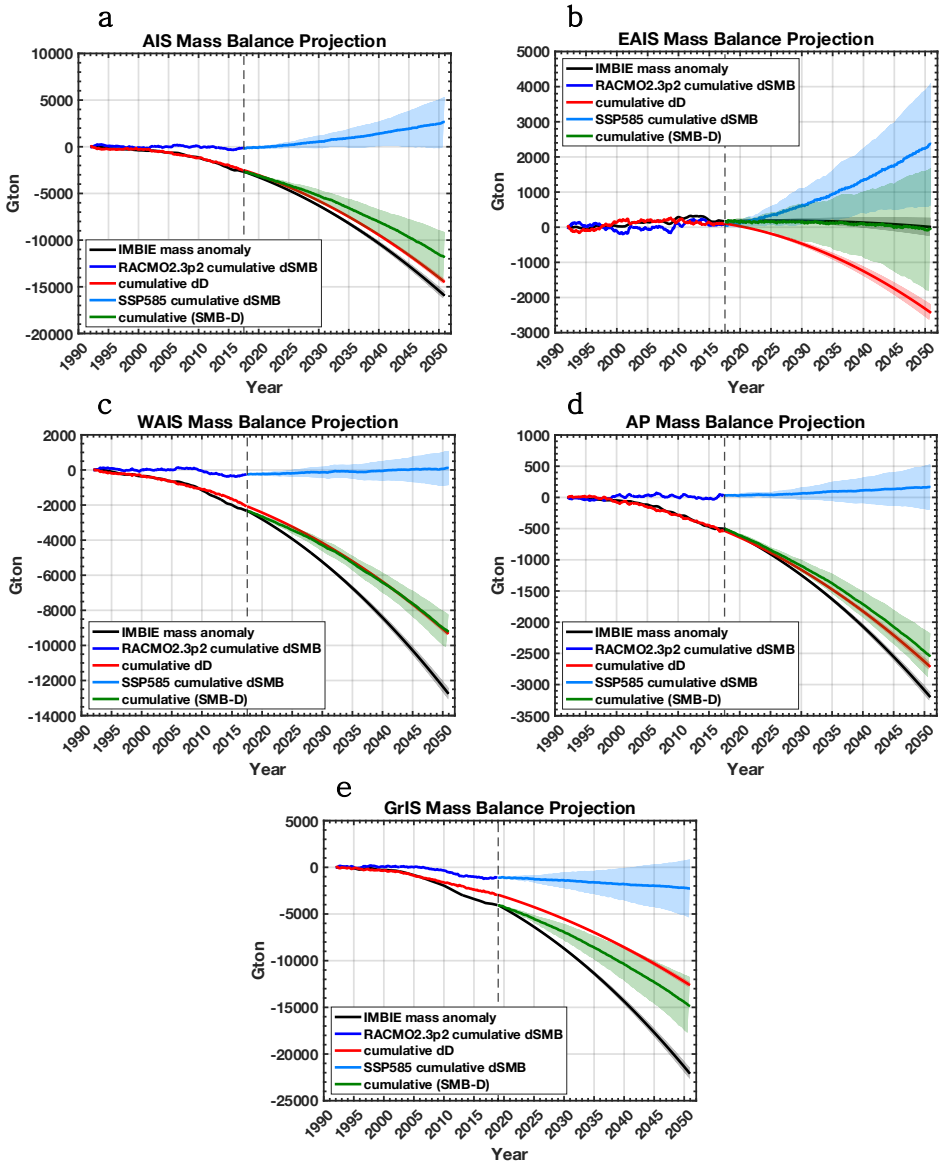

Figure 5. Similar to Figure 4 except for the CMIP6 SMB model in the SSP585 scenario.

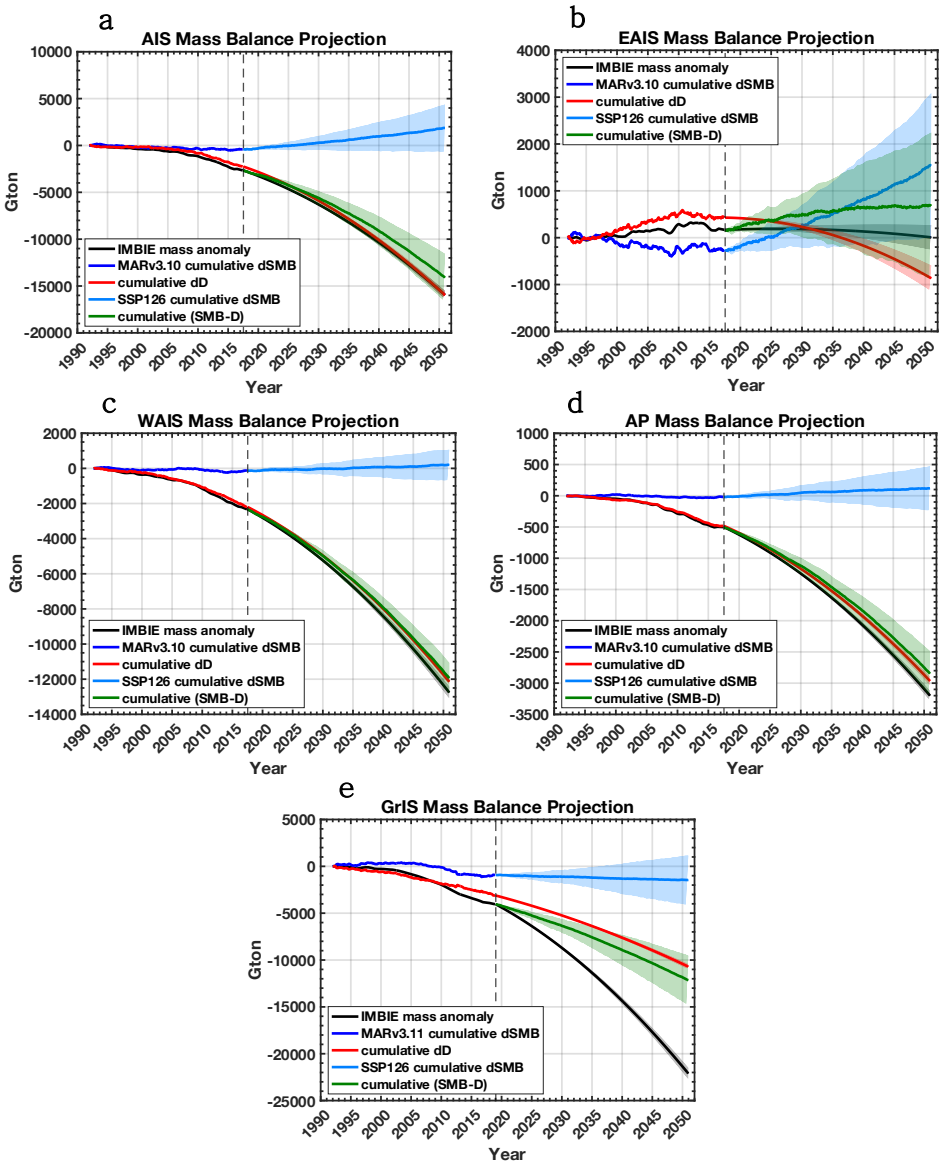

Figure 6. Similar to Figure 4 except for MARv3.11 SMB reanalysis.

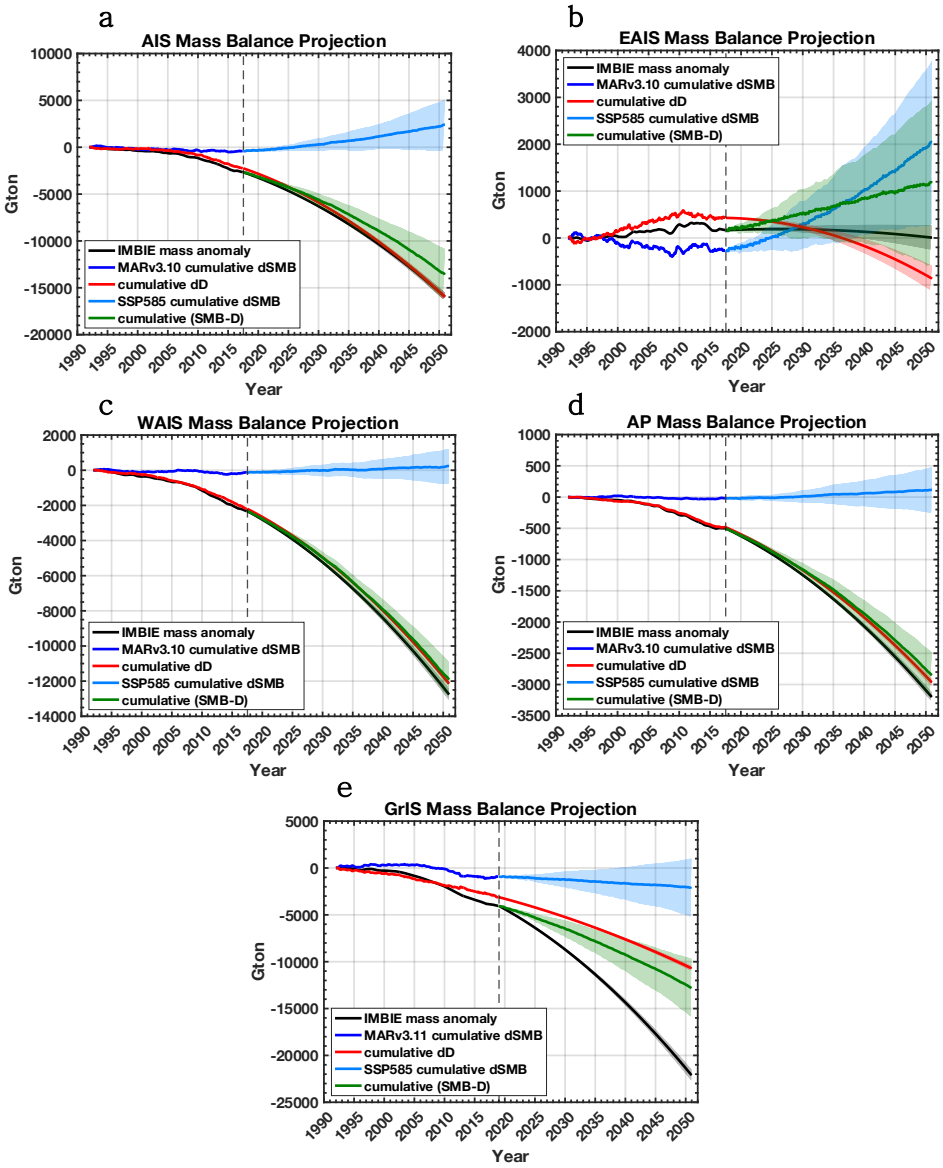

Figure 7. Similar to Figure 6 except for the CMIP6 SMB model in the SSP585 scenario.

Unit: [Gton]		AIS	EAIS	WAIS	AP	GrIS
RACMO	SSP126	-12367±2515	-568±1558	-9256±872	-2543±357	-14232±2615
	SSP585	-11846±2704	-68±1756	-9230±989	-2548±368	-14872±3113
MAR	SSP126	-14103±2530	679±1563	-11936±869	-2846±358	-12150±2611
	SSP585	-13581±2717	1179±1760	-11909±986	-2851±369	-12790±3110

Table 2. AIS and GrIS mass change projection from January 1992 to December 2050 (with 95% confidence intervals) estimated by cumulative $\int \delta SMB - \delta D$.

Chapter 5. Sea-Level Projections

Using future mass balance projections estimated in the previous chapter, we calculate SLFs according to water mass redistribution into oceans. The SLFs were estimated with the method in Section 2.2 to implement the realistic sea-level considering the influence of Earth's geoid change according to mass redistribution. Additionally, we also considered the geoid perturbation induced by changes in the Earth's rotational axis (due to the mass redistribution), named rotational feedback (Adhikari et al., 2019). As shown in Section 2.2, the mass balance projections should be converted into the mass balance on a grid ($\Delta\sigma(\theta,\phi)$). To do this, we divided the projected mass balance by the basin area of each ice sheet and assigned the value uniformly to the grids on the ice sheet.

Figures 8(a)~(d) show estimated SLFs induced by AIS mass change from December 2020 to December 2050. Four different SLFs are estimated based on using two SMBs (RACMO and MAR) for the historical period and two SMBs (SSP126 and SSP585) for 2020-2050. All of the SLFs show sea-level drops near WAIS and AP, due to the geoid decrease according to ice mass loss. On the other hand, the sea level rise far from AIS is predicted to be higher than GMSL. The projected GMSL rises vary from 23.55 mm to 29.79 mm. As implied in Table 2, the projections are largely different depending on the choice of reanalysis models. On the other hand, the choice of scenarios of the future SMB did not significantly influence to the sea-level projections.

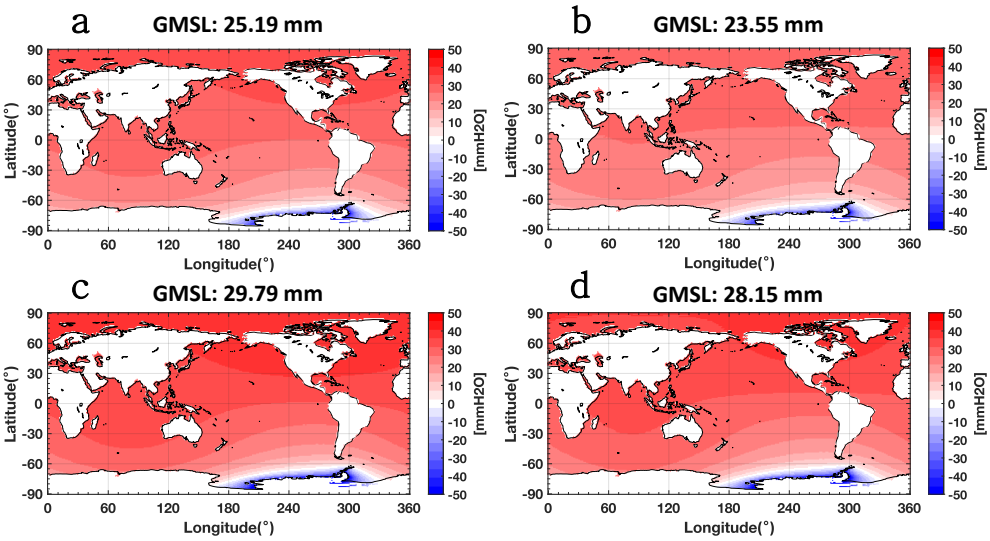

Figure 8. Regional sea-level projections difference from December 2020 to December 2050 calculated from the future AIS's mass balances estimated in this study. (a) SLF calculated from projected δM in both ice sheets using RACMO for historical SMB and CMIP6 SSP126 scenario SMB for future SMB. (b) similar to (a) except using SSP585 scenario. (c) similar to (a) except using MAR. (d) estimates with MAR and SSP585.

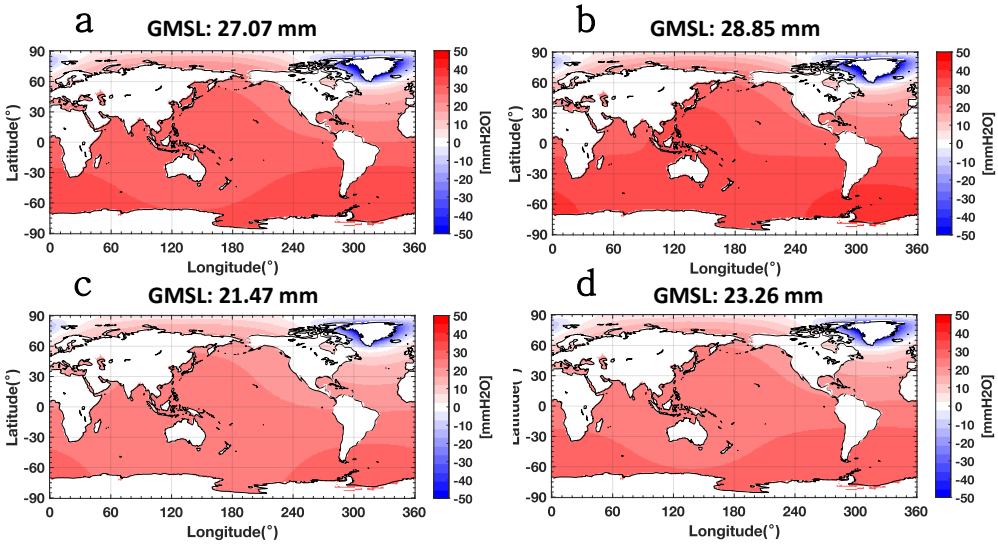

Figure 9. Similar to Figure 8 but using the projections of the GrIS' mass balance

The SLFs estimated by ice mass change from December 2020 to December 2050 in GrIS in shown in Figure 9. As similarly shown in Figure 8, the significant sea-level drops are expected near the GrIS, while higher sea-level rise are expected in the region far from GrIS. The GMSL rise induced by ice mass loss in GrIS ranges from 21.47 mm to 28.85 mm.

Total sea-level projections estimated from AIS and GrIS are shown in Figure 10. The spatial patterns of SLF show sea-level drop near both ice sheet regions and higher sea-level rises (than GMSL) in open oceans. The projected GMSL due to AIS and GrIS ranges from 51.26 mm to 52.40 mm.

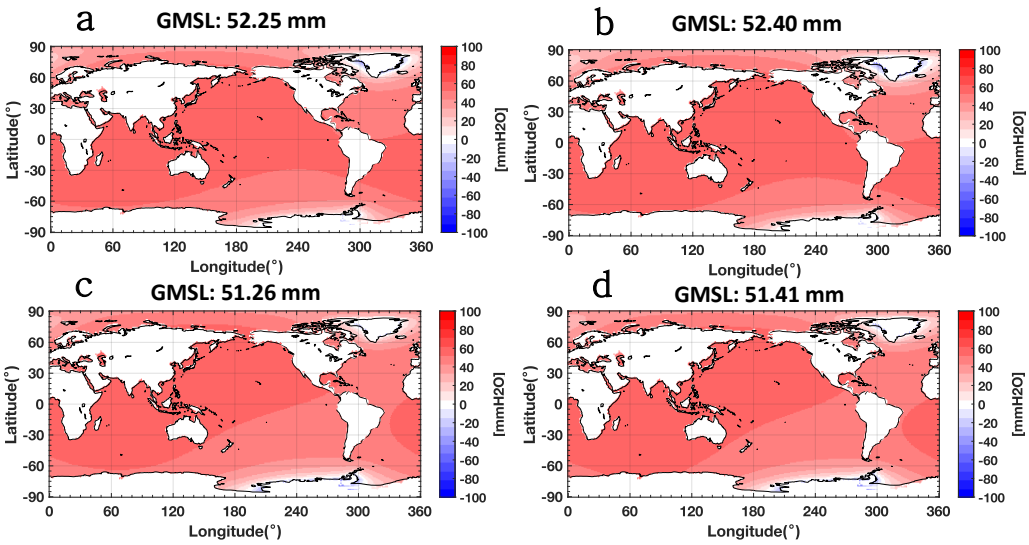

Figure 10. SLFs associated with both ice sheets (sum of Figures 8 and 9).

Chapter 6. Discussion and Conclusions

AIS and GrIS ice mass changes are expected to be the major contributors to the future GMSL rise. Ice sheet models have been used to predict AIS and GrIS mass changes to understand future GMSL rise, but there are significant disagreements among model prediction.

In this study, we estimated future AIS and GrIS mass changes empirically based on the fact that ice dynamic effect on ice sheet mass balances varies multi-decadal or longer time scale. Therefore, we assume that a linear trend and acceleration components of ice discharge variations in contemporary AIS and GrIS mass change would continue to the next several decades. The two components in AIS and GrIS were estimated from the difference between ice sheets mass balance observed by multiple remote sensing and surface mass balance from regional climate models. Using the estimated linear and acceleration components, cumulative ice discharge was projected up to 2050. Future projection of surface mass balance was also added to the ice discharge projection to estimate future ice mass variations and subsequent sea level changes.

We found that ice mass changes in AIS would be decreased mostly by increase in ice discharge in WAIS and AP. In the case of GrIS, significant ice mass loss is expected as well, due to the combined effect of SMB and ice discharge increase. Large SMB discrepancies in CMIP6 models would be the major uncertainty of this estimates.

By implementing SLFs, we suggested more realistic sea-level projections. GMSL rise due to ice mass loss is estimated to be about 23.55 - 29.79 mm for AIS and about 21.47 - 28.85 mm for GrIS. In

total, GMSL rise due to two ice sheets would be about 51.26 - 52.40 mm. These estimates are within the range of predictions from model simulations, about 10-80mm for AIS and 20-40mm for GrIS (Masson-Delmotte et al., 2021).

The SLFs suggest that there will be sea-level drops near both ice sheet region, but a higher sea level is expected in the regions far from the ice sheets, where most of the humans live. Therefore, the result of this study will be important for mankind in coping with future sea-level rise.

Reference

Adhikari, S., Ivins, E. R., Frederikse, T., Landerer, F. W., & Caron, L. (2019). Sea-level fingerprints emergent from GRACE mission data. *Earth Syst. Sci. Data, 11*(2), 629-646. https://essd.copernicus.org/articles/11/629/2019/

Chen, X., Zhang, X., Church, J. A., Watson, C. S., King, M. A., Monselesan, D., et al. (2017). The increasing rate of global mean sea-level rise during 1993–2014. *Nature Climate Change, 7*(7), 492-495. https://doi.org/10.1038/nclimate3325

Diener, T., Sasgen, I., Agosta, C., Fürst, J. J., Braun, M. H., Konrad, H., & Fettweis, X. (2021). Acceleration of Dynamic Ice Loss in Antarctica From Satellite Gravimetry. *Frontiers in Earth Science, 9*. Original Research. https://www.frontiersin.org/article/10.3389/feart.2021.741789

Eyring, V., Bony, S., Meehl, G. A., Senior, C. A., Stevens, B., Stouffer, R. J., & Taylor, K. E. (2016). Overview of the Coupled Model Intercomparison Project Phase 6 (CMIP6) experimental design and organization. *Geosci. Model Dev., 9*(5), 1937-1958. https://gmd.copernicus.org/articles/9/1937/2016/

Farrell, W. E., & Clark, J. A. (1976). On Postglacial Sea Level. *Geophysical Journal of the Royal Astronomical Society, 46*(3), 647-667.

Fettweis, X. (2022). *Modèle Atmosphérique Régional (MAR) version 3.11 regional climate model output, 1979-2019, Greenland domain, 10 kilometer (km) horizontal resolution.*

Goelzer, H., Nowicki, S., Payne, A., Larour, E., Seroussi, H., Lipscomb, W. H., et al. (2020). The future sea-level contribution of the Greenland ice sheet: a multi-model ensemble study of ISMIP6. *The Cryosphere, 14*(9), 3071-3096. https://tc.copernicus.org/articles/14/3071/2020/

Kim, B.-H., Seo, K.-W., Eom, J., Chen, J., & Wilson, C. R. (2020). Antarctic ice mass variations from 1979 to 2017 driven by anomalous precipitation accumulation. *Scientific Reports, 10*(1), 20366. https://doi.org/10.1038/s41598-020-77403-5

Kim, J.-S., Seo, K.-W., Jeon, T., Chen, J., & Wilson, C. R. (2019). Missing Hydrological Contribution to Sea Level Rise. *Geophysical Research Letters, 46*(21), 12049-12055. https://doi.org/10.1029/2019GL085470. https://doi.org/10.1029/2019GL085470

Llovel, W., Purkey, S., Meyssignac, B., Blazquez, A., Kolodziejczyk, N., & Bamber, J. (2019). Global ocean freshening, ocean mass increase and global mean sea level rise over 2005–2015. *Scientific Reports, 9*(1), 17717. https://doi.org/10.1038/s41598-019-54239-2

Mankoff, K. D., Fettweis, X., Langen, P. L., Stendel, M., Kjeldsen, K. K., Karlsson, N. B., et al. (2021). Greenland ice sheet mass balance from 1840 through next week. *Earth Syst. Sci. Data, 13*(10), 5001-5025. https://essd.copernicus.org/articles/13/5001/2021/

Masson-Delmotte, V., P. Z., A. Pirani, S.L. Connors, C. Péan, S. Berger, et al. (2021). *IPCC, 2021: Climate Change 2021: The Physical Science Basis. Contribution of Working Group I to the Sixth Assessment Report of the Intergovernmental Panel on Climate Change*. Retrieved from Cambridge University Press:

Mitrovica, J. X., Tamisiea, M. E., Davis, J. L., & Milne, G. A. (2001). Recent mass balance of polar ice sheets inferred from patterns of global sea-level change. *Nature, 409*(6823), 1026-1029. https://www.ncbi.nlm.nih.gov/pubmed/11234008

Mottram, R., Hansen, N., Kittel, C., van Wessem, J. M., Agosta, C., Amory, C., et al. (2021). What is the surface mass balance of Antarctica? An intercomparison of regional climate model estimates. *The Cryosphere, 15*(8), 3751-3784. https://tc.copernicus.org/articles/15/3751/2021/

Mouginot, J., Rignot, E., Bjørk, A. A., van den Broeke, M., Millan, R., Morlighem, M., et al.

(2019). Forty-six years of Greenland Ice Sheet mass balance from 1972 to 2018. *Proceedings of the National Academy of Sciences, 116*(19), 9239. http://www.pnas.org/content/116/19/9239.abstract

Noël, B., van de Berg, W. J., Lhermitte, S., & van den Broeke, M. R. (2019). Rapid ablation zone expansion amplifies north Greenland mass loss. *Science Advances, 5*(9), eaaw0123. http://advances.sciencemag.org/content/5/9/eaaw0123.abstract

Noël, B., van de Berg, W. J., van Meijgaard, E., Kuipers Munneke, P., van de Wal, R. S. W., & van den Broeke, M. R. (2015). Evaluation of the updated regional climate model RACMO2.3: summer snowfall impact on the Greenland Ice Sheet. *The Cryosphere, 9*(5), 1831-1844. https://tc.copernicus.org/articles/9/1831/2015/

Noël, B., van de Berg, W. J., van Wessem, J. M., van Meijgaard, E., van As, D., Lenaerts, J. T. M., et al. (2018). Modelling the climate and surface mass balance of polar ice sheets using RACMO2 – Part 1: Greenland (1958–2016). *The Cryosphere, 12*(3), 811-831. https://tc.copernicus.org/articles/12/811/2018/

Seo, K.-W., Wilson, C. R., Scambos, T., Kim, B.-M., Waliser, D. E., Tian, B., et al. (2015). Surface mass balance contributions to acceleration of Antarctic ice mass loss during 2003–2013. *Journal of Geophysical Research: Solid Earth, 120*(5), 3617-3627. https://doi.org/10.1002/2014JB011755. https://doi.org/10.1002/2014JB011755

Seroussi, H., Nowicki, S., Payne, A. J., Goelzer, H., Lipscomb, W. H., Abe-Ouchi, A., et al. (2020). ISMIP6 Antarctica: a multi-model ensemble of the Antarctic ice sheet evolution over the 21st century. *The Cryosphere, 14*(9), 3033-3070. https://tc.copernicus.org/articles/14/3033/2020/

Shepherd, A., Ivins, E., Rignot, E., Smith, B., van den Broeke, M., Velicogna, I., et al. (2018). Mass balance of the Antarctic Ice Sheet from 1992 to 2017. *Nature, 558*(7709), 219-222. https://doi.org/10.1038/s41586-018-0179-y

Shepherd, A., Ivins, E., Rignot, E., Smith, B., van den Broeke, M., Velicogna, I., et al. (2020). Mass balance of the Greenland Ice Sheet from 1992 to 2018. *Nature, 579*(7798), 233-239. https://doi.org/10.1038/s41586-019-1855-2

van den Broeke, M., Bamber, J., Ettema, J., Rignot, E., Schrama, E., van de Berg, W. J., et al. (2009). Partitioning Recent Greenland Mass Loss. *Science, 326*(5955), 984. http://science.sciencemag.org/content/326/5955/984.abstract

Van Wessem, J. M., Reijmer, C. H., Morlighem, M., Mouginot, J., Rignot, E., Medley, B., et al. (2014). Improved representation of East Antarctic surface mass balance in a regional atmospheric climate model. *Journal of Glaciology, 60*(222), 761-770. https://www.cambridge.org/core/article/improved-representation-of-east-antarctic-surface-mass-balance-in-a-regional-atmospheric-climate-model/696B69305FDF44A9CD1BD770F61E4174

Wahr, J., Molenaar, M., & Bryan, F. (1998). Time variability of the Earth's gravity field: Hydrological and oceanic effects and their possible detection using GRACE. *Journal of Geophysical Research: Solid Earth, 103*(B12), 30205-30229. https://agupubs.onlinelibrary.wiley.com/doi/abs/10.1029/98JB02844

Wessem, J. M., Berg, W. J., Noël, B., Meijgaard, E., Amory, C., Birnbaum, G., et al. (2018). Modelling the climate and surface mass balance of polar ice sheets using RACMO2 – Part 2: Antarctica (1979–2016). *The Cryosphere, 12*, 1479-1498.

Wouters, B., Gardner, A. S., & Moholdt, G. (2019). Global Glacier Mass Loss During the GRACE Satellite Mission (2002-2016). *Frontiers in Earth Science, 7*. Original Research. https://www.frontiersin.org/article/10.3389/feart.2019.00096

Xu, Z., Schrama, E. J. O., van der Wal, W., van den Broeke, M., & Enderlin, E. M. (2016). Improved GRACE regional mass balance estimates of the Greenland ice sheet cross-validated with the input–output method. *The Cryosphere, 10*(2), 895-912. https://tc.copernicus.org/articles/10/895/2016/

국문초록

남극과 그린란드 얼음 질량 변화에 의한 2050 년 전 지구 해수면 변화 추정

서울대학교 대학원
과학교육과 지구과학 전공
이 동 혁

남극과 그린란드 빙상에 의한 전 지구 평균 해수면 상승은 지구온난화의 중요한 신호이다. 해수면 상승률이 대체로 남극과 그린란드 빙상 질량 감소에 의해 결정되기 때문에, 미래의 남극과 그린란드 빙상의 질량 변화를 예측하는 것이 무엇보다 중요하다. 여러 빙상 모델들이 남극과 그린란드의 미래 빙상 질량 변화와 이에 따른 해수면 변화를 예측하고 있지만 예측치에 큰 편차가 있다. 본 연구에서는 빙하 유출량이 향후 몇 십년간 일정하게 변화할 것이라는 가정을 바탕으로 계산한 과거 빙하 유출량의 선형성분과 가속성분을 이용하여 2050 년 까지의 남극과 그린란드 빙상 질량 변화를 계산하였다. 여기서 빙하 유출량의 각 성분들은 표면 질량 변화 효과를 보정한 빙상 질량 변화의 관측값을 통해 추정하였다. 미래 표면 질량 변화값 역시 기후 모델들의 미래 예측값을 바탕으로 포함시켰다. 결론적으로 남극 빙상 질량 변화에 의한 해수면 변화율은 0.79~0.99 mm/yr 이며 그린란드 빙상 질량 변화에 의한 해수면 변화율은 0.72 ~ 0.96 mm/yr 로 예측되었다. 남극과 그린란드의 미래 해수면 상승에 대한 기여도는

비슷하거나 남극이 조금 큰 것으로 예측되었다. 여러 기후모델들 간 표면 질량 변화의 큰 편차는 본 연구의 주요 불확실성이라고 볼 수 있다.

주요 용어 : 얼음 질량 변화, 남극, 그린란드, 미래 해수면 상승 예측

학번 : 2020-21076